Semaphorin signaling via MICAL3 induces symmetric cell division to expand breast cancer stem-like cells

Kana Tominaga[a,b,c,1,2], Hiroshi Minato[d,3], Takahiko Murayama[a], Asako Sasahara[a,e], Tatsunori Nishimura[c], Etsuko Kiyokawa[d], Hajime Kanauchi[f], Seiichiro Shimizu[g], Ayaka Sato[e], Kotoe Nishioka[e], Ei-ichi Tsuji[e], Masao Yano[h], Toshihisa Ogawa[e], Hideshi Ishii[i], Masaki Mori[j], Koichi Akashi[k], Koji Okamoto[b], Masahiko Tanabe[e], Kei-ichiro Tada[e,4], Arinobu Tojo[a,c], and Noriko Gotoh[a,c,1]

[a]Division of Molecular Therapy, Institute of Medical Science, University of Tokyo, Tokyo 108-8639, Japan; [b]Division of Cancer Differentiation, National Cancer Center Research Institute, Tokyo 104-0045, Japan; [c]Division of Cancer Cell Biology, Cancer Research Institute, Kanazawa University, Kanazawa City, Ishikawa 920-1192, Japan; [d]Department of Pathology and Laboratory Medicine, Kanazawa Medical University, Uchinada-Machi, Ishikawa 920-0265, Japan; [e]Department of Breast and Endocrine Surgery, Graduate School of Medicine, University of Tokyo, Tokyo 112-8655, Japan; [f]Department of Breast and Endocrine Surgery, Showa General Hospital, Kodaira City, Tokyo 187-8510, Japan; [g]Department of Pathological Diagnosis, Showa General Hospital, Kodaira City, Tokyo 187-8510, Japan; [h]Department of Surgery, Minami-Machida Hospital, Machida City, Tokyo 194-0004, Japan; [i]Department of Medical Data Science, Osaka University Graduate School of Medicine, Suita City, Osaka 565-0871, Japan; [j]Department of Gastroenterological Surgery, Osaka University Graduate School of Medicine, Suita City, Osaka 565-0871, Japan; and [k]Department of Medicine and Biosystemic Science, Graduate School of Medical Sciences, Kyushu University, Fukuoka 812-8582, Japan

Cancer stem-like cells (CSCs) are expanded in the CSC niche by increased frequency of symmetric cell divisions at the expense of asymmetric cell divisions. The symmetric division of CSCs is important for the malignant properties of cancer; however, underlying molecular mechanisms remain largely elusive. Here, we show a cytokine, semaphorin 3 (Sema3), produced from the CSC niche, induces symmetric divisions of CSCs to expand the CSC population. Our findings indicate that stimulation with Sema3 induced sphere formation in breast cancer cells through neuropilin 1 (NP1) receptor that was specifically expressed in breast CSCs (BCSCs). Knockdown of *MICAL3*, a cytoplasmic Sema3 signal transducer, greatly decreased tumor sphere formation and tumor-initiating activity. Mechanistically, Sema3 induced interaction among MICAL3, collapsin response mediator protein 2 (CRMP2), and Numb. It appears that activity of MICAL3 monooxygenase (MO) stimulated by Sema3 is required for tumor sphere formation, interaction between CRMP2 and Numb, and accumulation of Numb protein. We found that knockdown of *CRMP2* or *Numb* significantly decreased tumor sphere formation. Moreover, *MICAL3* knockdown significantly decreased Sema3-induced symmetric divisions in NP1/Numb-positive BCSCs and increased asymmetric division that produces NP1/Numb negative cells without stem-like properties. In addition, breast cancer patients with NP1-positive cancer tissues show poor prognosis. Therefore, the niche factor Sema3-stimulated NP1/MICAL3/CRMP2/Numb axis appears to expand CSCs at least partly through increased frequency of MICAL3-mediated symmetric division of CSCs.

neuropilin | semaphorin | breast cancer | tumor micoenvironment | cancer stem cell niche

Breast cancer is the most common type of cancer among women throughout the world (1). The increasing rate of mortality due to breast cancer raises serious problems. Recent evidence indicates that tumor tissues are composed of heterogeneous cell populations including a relatively small number of cancer stem-like cells (CSCs) and other differentiated cancer cells (2). CSCs tend to survive irrespective of conventional chemotherapy, radiotherapy, and following treatment with molecular targeted drugs, because these treatment strategies target rapidly proliferating differentiated cancer cells but not CSCs. Targeting CSCs is thus important to improve the prognosis of cancer patients; however, molecular targeting drugs against CSCs are still unmet needs.

Stem cells have the ability to self-renew and differentiate. A stem cell divides into two daughter cells using one of two types of cell division: symmetric and asymmetric (3, 4). With symmetric division, a stem cell produces two identical daughter cells and doubles the number of self-renewing stem cells. In contrast, asymmetric cell division gives rise to two different daughter cells: one differentiated cell and one self-renewing stem cell. Recent evidence suggests that CSCs have similar characteristics regarding cell division (4, 5). Researchers believe that the more CSCs become malignant, the more they have a tendency to divide symmetrically, producing two daughter CSCs and leading to expansion of the CSC population. The molecular mechanisms of how each type of CSC division is determined remain obscure. If the mechanisms are clarified, a novel strategy for cancer therapy

Significance

Tumors are composed of both cancer stem-like cells (CSCs) and differentiated cancer cells. Each CSC can undergo either a symmetric cell division to produce two CSCs or an asymmetric cell division to produce one CSC and one differentiated cancer cell. It is believed that the rate of symmetric division increases as more CSCs become malignant; however, underlying molecular mechanisms remain elusive. Here we show that stimulation with a cytokine, semaphorin (Sema), activates monooxygenase of MICAL3, a cytoplasmic signal transducer, through the neuropilin (NP) receptor that is specifically expressed on the breast CSC plasma membrane. The activation of MICAL3 induces symmetric division of CSCs. Each molecule in this signaling pathway represents a promising therapeutic target for eliminating CSCs.

www.manaraa.com

MEDICAL SCIENCES

may be established to reduce the CSC population by inhibiting symmetric division of CSCs.

In tumor tissues, CSCs are surrounded by a variety of cell types, including differentiated cancer cells and endothelial cells that comprise blood vessels (6). All these cells create a microenvironment that is called the CSC niche. CSCs are thought to survive by utilizing the CSC niche. We and other researchers previously showed that breast cancer stem-like cells (BCSCs) maintain stemness for their survival in the inflammatory microenvironment by utilizing growth factors or cytokines that are produced by cancer cells in the CSC niche (6–9). By systematically analyzing the gene expression profile via activation of NF-κB, the inflammatory master transcription factor complex, stimulated by the growth factor heregulin (HRG), we identified several CSC niche factors that are involved in maintenance of stemness of CSCs, including insulin-like growth factor 2 (IGF2) and growth differentiation factor 15 (10, 11). A gene encoding the cytokine Sema3B was among the top genes in the list, and expression levels of *MICAL3* were up-regulated (10).

The Sema family of membrane-bound or secreted proteins comprises 20 members in vertebrates (12). The type 3 Semas, including Sema3A and Sema3B, are secreted proteins that were originally discovered as ligands that relay repulsive signals for axon guidance during development of neuronal tissues in brain (13). Sema3A and Sema3B were subsequently shown to be involved in tumorigenesis in a context-dependent manner (14). NP and Plexin form a receptor complex for Semas (15). NP serves as the primary receptor for ligand binding, whereas the Plexin coreceptor transduces the Sema signal via the intracellular domain and activates MICAL.

MICAL is a cytoplasmic multidomain signaling protein that consists of a flavin adenine dinucleotide (FAD)-containing monooxygenase (MO) domain at the N terminus and domains for interacting with multiple proteins (16). The MICAL family of proteins comprises three major members in vertebrates: MICAL1, MICAL2, and MICAL3. MICALs have several functions that include axon repulsion via formation of a complex with CRMP (17). CRMP2 binds to tubulin heterodimers and induces microtubule polymerization (12). When Sema binds to NP, the MO domain in MICAL is activated and generates H_2O_2, a reactive oxygen species (ROS) (18). Then, CRMP2 homodimers are formed with intermolecular S–S bonds at Cys^{504} through oxidation, leading to the repulsion of axons (19).

CRMP2 binds to several other proteins, including Numb in neurons (20). During axonal growth, CRMP2-bound Numb is involved in endocytosis at the growth cone. Numb also plays an important role in regulation of symmetric–asymmetric division of neural cells (21, 22). In *Drosophila* neural cells, Numb is expressed in differentiated cells and regulates asymmetric cell division (23), whereas in mammalian neural cells, Numb protein is expressed in dividing stem or progenitor cells (24, 25).

In this study, we provide evidence that Sema acts as a CSC niche factor and stimulates NP/MICAL3/CRMP2/Numb axis, leading to symmetric division and expansion of BCSCs.

Results

The Sema3-NP Receptor Axis Plays Important Roles in BCSCs in Vitro.

We first examined whether the Sema3 signaling plays roles for stem-like properties of breast cancer cells (BCCs). The tumor sphere-forming ability measures properties of CSCs in vitro (26). Sphere culture medium (SCM), that contains a mixture of several growth factors or hormones, is usually used to form tumor spheres. We found that recombinant Sema3A induced tumor sphere formation of BCCs, as a single cytokine, without other growth factors or hormones (Fig. 1 *A* and *B*). To analyze the activation of Sema3 signaling through NP1, a receptor for Sema3A, we studied the expression of NP1. Compared with MCF10A (a normal human mammary epithelial cell line), NP1 expression was elevated in all of the breast cancer cell lines that we examined (Fig. 1*C*). *NP1* expression was higher in breast cancer tissues than in normal breast tissues in the Oncomine database (https://www.oncomine.org/resource/login.html) (*SI Appendix*, Fig. S1). Plexin A, another receptor for Sema3, is expressed at similar levels in MCF10A and human breast cancer cell lines (27). The $CD24^{-/low}/CD44^{high}$ cell population is known to be enriched by BCSCs (28). Tumor sphere formation, induced by SCM, was observed in the $CD24^{-/low}/CD44^{high}$ patient-derived BCSC-enriched population, but not in the $CD24^{-/low}/CD44^{-/low}$ non-BCSC population, as reported previously (8) (*SI Appendix*, Fig. S2). NP1 was expressed at higher levels in the $CD24^{-/low}/CD44^{high}$ patient-derived BCSC-enriched population than in the $CD24^{-/low}/CD44^{-/low}$ non-BCSC population (Fig. 1 *D* and *E* and *SI Appendix*, Fig. S3). Tumor sphere formation of patient-derived BCCs significantly decreased in the presence of an NP1 neutralizing antibody in SCM (Fig. 1 *F* and *G*). We then sorted patient-derived BCCs using an anti-NP1

Fig. 1. Sema3A stimulation and the highly NP1-positive cell population show strong tumor sphere-forming ability. (*A*) Representative phase contrast images of tumor sphere formation in luminal type MCF7 cells and basal type BT20 cells cultured in DMEM/F12 with or without human recombinant Sema3A alone. (*B*) Quantification of tumor sphere formation by treatment with Sema3A; $n = 4$. (*C*) Expression of NP1 protein with immunoblotting. (*D*) FACS analysis of freshly obtained patient-derived BCCs (patient 5). The cells were sorted according to the expression of CD44 and CD24 and then sorted according to the expression of NP1. (*E*) Percentages of NP1^{high} cells in the CD44^{high}/CD24$^{-/low}$ BCSC-enriched population or control non-BCSC populations. BCCs derived from three patients (patients 4, 5, and 8) were used. (*F*) Representative phase contrast images of tumor sphere formation in patient-derived BCCs (patient 9) in the presence or absence of an anti-NP1 neutralizing antibody (NP1 NAb) or control IgG in SCM. (Scale bar: 100 μm.) (*G*) Quantification of the tumor sphere-forming ability of patient-derived BCCs in SCM. Tumor sphere-forming ability was significantly reduced by treatment with NP1 Nab or control IgG; $n = 4$. (*H*) FACS analysis of freshly obtained patient-derived BCCs (patient 7). The cells were sorted according to the expression of NP1. (*I*) Representative phase contrast images of tumor sphere formation by patient-derived BCCs. (Scale bar: 100 μm.) (*J*) Highly NP1^{high} cells but not NP1$^{-/low}$ cells of patient-derived BCCs (patient 5) formed tumor spheres by 200 ng/mL Sema3A stimulation; $n = 4$. (*K*) Expression of *Nanog*, *ALDH1*, and *cytokeratin 18* (*CK18*) mRNA with quantitative real-time (qRT)-PCR between NP1^{high} cells and NP1$^{-/low}$ cells in patient-derived BCCs; $n = 4$. Data are shown as mean ± SD. *$P < 0.05$, **$P < 0.01$, ***$P < 0.001$ by Student's t tests.

www.manaraa.com
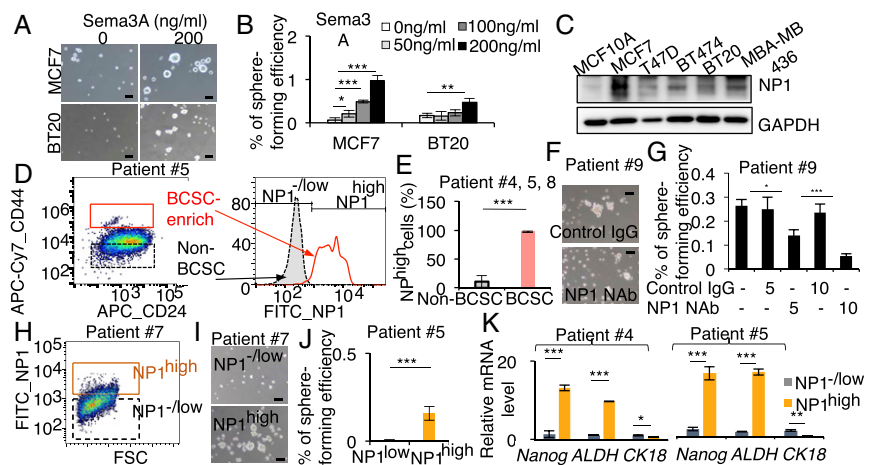
antibody (Fig. 1*H*). We found that the NP1^{high} cell population, but not the NP1$^{-/low}$ cell population, gave rise to tumor spheres either in Sema3A-containing medium (Fig. 1 *I* and *J*) or in SCM (*SI Appendix*, Fig. S4). In contrast, when patient-derived BCCs were sorted using an anti-Plexin A4 antibody to obtain cell populations with either high or low levels of Plexin A4 expression (*SI Appendix*, Fig. S5), both populations formed tumor spheres with similar efficiency. It is possible that other Plexin family proteins are expressed in these cells. The stemness markers *Nanog* and *ALDH1* were expressed at higher levels, whereas the differentiation marker *Cytokeratin18* (*CK18*) was expressed at lower levels in the NP1^{high} cell population than in the NP1$^{-/low}$ cell population (Fig. 1*K*). These results suggest that Sema3A induces tumor sphere formation through NP1 receptor that is enriched in the BCSC population and that the Sema3-NP1 axis is required for efficient tumor sphere formation in SCM. Thus, NP1 would be a novel functional marker for BCSCs. In addition, we performed immunohistochemistry to examine in which cell types Sema3A and NP1 are expressed by using breast cancer tissues. Sema3A was stained in tumor cells, but not in endothelial cells or stroma cells, whereas NP1 was stained in tumor cells and endothelial cells, but not in stroma cells (*SI Appendix*, Fig. S6).

MICAL3 Plays a Critical Role in BCSCs. MICAL plays a central role in Sema-NP1–stimulated axon repulsion signaling in the nervous system (16). *MICAL3* expression was higher in breast cancer tissues than in normal breast tissues in the Oncomine database (Fig. 2*A*). The breast cancer patients with higher levels of *MICAL3* expression showed worse outcomes than those expressing lower levels of *MICAL3* in the gene expression profiles (Fig. 2*B*). The tumor sphere-forming ability was significantly decreased by *MICAL3* knockdown in BCCs (*SI Appendix*, Fig. S7*A*) cultured either in SCM (Fig. 2 *C–E*) or in Sema3A-containing medium (*SI Appendix*, Fig. S8). We also performed in vitro limiting dilution assay (LDA) for tumor sphere formation in patient-derived BCCs using two different shRNAs for *MICAL3*. *MICAL3* knockdown significantly decreased tumor sphere-forming ability (*SI Appendix*, Figs. S7*B* and S9). However, it did not significantly affect proliferation of BCCs cultured in adherent condition in 10% serum-containing medium (*SI Appendix*, Fig. S10). Tumor-initiating activity measures properties of CSCs in vivo (26). We next analyzed a patient-derived xenograft (PDX) model in which patient-derived BCCs were inoculated into the mammary fat pads of immunodeficient mice. The tumor-initiating activity was markedly decreased in *MICAL3* knockdown cells (Fig. 2 *F* and *G* and *SI Appendix*, Fig. S7*B*). These findings suggest that MICAL3 plays a critical role in BCSCs in vitro and in vivo.
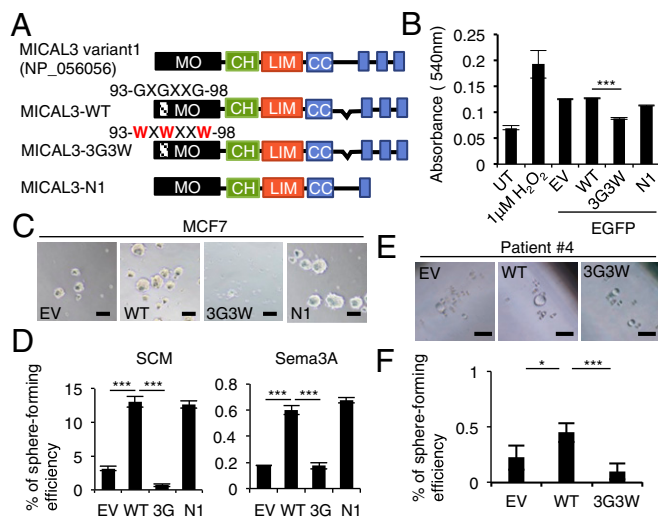
MO Domain of MICAL3 Plays Critical Roles in the Tumor Sphere-Forming Ability. MICAL3 includes a FAD-containing MO domain, a calponin homology (CH) domain, a LIM domain, and a coiled-coil (CC) domain (Fig. 3*A*) (29). To determine which of these domains is required for tumor sphere formation in BCCs, we used cDNA constructs, MICAL3-wild type (WT), MICAL3-3G3W and MICAL3-N1 (Fig. 3*A*). MICAL3-3G3W is a MICAL3 mutant in which the three glycines in the FAD-binding motif GXGXXG were mutated to tryptophan, resulting in a defect in MO activity. Expression of MICAL3-3G3W abrogates the function of *Drosophila* MICAL in axon guidance and actin disassembly (30). MICAL3-N1 lacks the C-terminal region, which contributes to vesicle fusion to the plasma membrane (31). We transfected each construct into HEK293T cells and measured levels of H_2O_2 production (18, 32, 33). As expected, cells transfected with MICAL3-3G3W produced significantly lower levels of H_2O_2 than those with MICAL3-WT or MICAL3-N1 (Fig. 3*B*), indicating that the MO domain but not the C-terminal region of MICAL3 is required for production of H_2O_2. We next analyzed tumor sphere formation in BCCs that were transiently transfected with those constructs. When
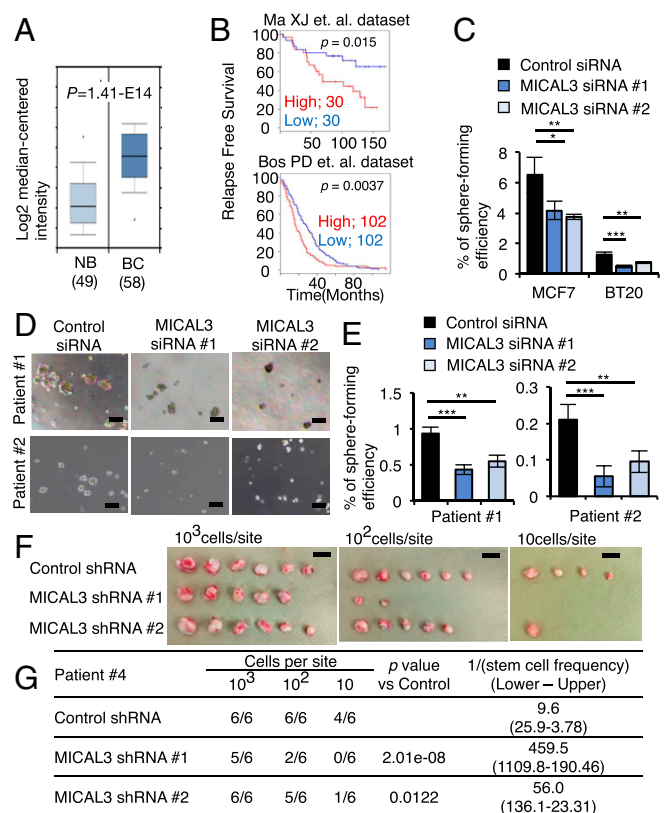
Fig. 2. MICAL3 is a key factor for tumor sphere formation by human BCCs. (*A*) Comparison of expression levels of *MICAL3* mRNA in normal breast (NB) and breast cancer (BC) tissues using Oncomine databases. (*B*) Kaplan–Meier analysis of relapse-free survival of patients with breast cancer tissues showing low or high *MICAL3* expression. Median was used for cutoff values. Gene expression profiles GSE1379 (*Upper*) and GSE12276 (*Lower*) were used for analysis. (*C*) Cells were cultured in SCM that contains several growth factors and hormones (epidermal growth factor, basic fibroblast growth factor, and B27) in DMEM/F12. SCM-induced tumor sphere formation was decreased by *MICAL3* knockdown; *n* = 4. (*D*) Representative phase contrast images of tumor sphere formation by *MICAL3* knockdown in patient-derived BCCs (patients 1 and 2). (Scale bar: 100 μm.) (*E*) SCM-induced tumor sphere formation was decreased by *MICAL3* knockdown in patient-derived BCCs; *n* = 4. (*F*) Representative images of tumors generated in mice injected with patient-derived BCCs (patient 4). (Scale bar: 1 cm.) (*G*) The 10^3, 10^2, or 10 cells per site were s.c. injected into the mammary fat pads of 8-wk-old female immunodeficient mice. Results were obtained 60 d after implantation. Frequency determinations were generated using ELDA software (*SI Appendix*, Ref. 1). Data are shown as mean ± SD. *$P < 0.05$, **$P < 0.01$, ***$P < 0.001$ by Student's *t* tests. For LDAs, the method of Holm was used.

transfected cells were cultured in a floating condition, both MICAL3-WT– and MICAL3-N1–transfected cells were able to form more tumor spheres than empty vector (EV)-transfected cells either in SCM (Fig. 3 *C–F* and *SI Appendix*, Fig. S11 *A and B*) or in Sema3A-containing medium (Fig. 3*D*, *Right*). In contrast, the tumor sphere-forming ability was much lower in MICAL3-3G3W–transfected cells than in MICAL3-WT– or MICAL3-N1–transfected cells. These results suggest that the activity of MICAL3 MO is required for tumor sphere formation.

Sema3A-Stimulated MICAL3 MO Induces Interaction Between MICAL3 and CRMP2 and CRMP2 Dimerization in BCCs. MICAL-mediated H_2O_2 production contributes to CRMP2 interaction for axon repulsion (19). We next investigated the interaction between MICAL3 and CRMP2 using a Duolink in situ proximity ligation assay (PLA) (33). In situ PLA is a technique used to detect interactions between proteins inside a cell due to generation of

Tominaga et al.

MEDICAL SCIENCES

Fig. 3. MO domain of MICAL3 plays critical roles in tumor sphere formation. (*A*) Schematic of WT MICAL3 and mutant (3G3W and N1) constructs. (*B*) Measurement of H_2O_2 production using lysates of HEK293T cells transfected with the indicated constructs described in *A* in the presence of 200 μM NADPH. As a positive control, cells were treated with 1 μM H_2O_2; $n = 3$. (*C* and *E*) Representative phase contrast images of tumor sphere formation by MCF7 or patient-derived BCCs transiently transfected with the indicated constructs cultured in SCM. (Scale bar: 100 μm.) (*D* and *F*) Tumor sphere formation by MCF7 or patient-derived BCCs transfected with the indicated constructs cultured in SCM; $n = 3$. Data are shown as mean ± SD. *$P < 0.05$, ***$P < 0.001$ by Student's *t* tests.

fluorescent dots in images. We found that the number of PLA dots was greatly increased in BCCs in Sema3A-containing medium (*SI Appendix*, Fig. S12 *A* and *B*). We next examined whether the Sema3A-induced interaction between MICAL3 and CRMP2 occurs in NP1-positive or NP1-negative patient-derived BCCs using anti-NP1 antibody staining. We found that Sema3A treatment greatly increased PLA dots in NP1-positive cells (NP1^{posi}), but not so in NP1-negative cells (NP1^{nega}) (Fig. 4). These results suggest that Sema3A treatment induces interaction between MICAL3 and CRMP2 in human BCCs, especially in the NP1-positive cells. We next examined whether dimerization of CRMP2 is induced by Sema3A-stimulated activity of MICAL3 MO in BCCs. When we treated MCF7 cells with 1 μM H_2O_2 as a control and separated the total lysates with nonreducing SDS/PAGE, intensities of the bands around 135 kDa were found, corresponding to disulfide-linked homodimers of CRMP2, similarly observed in neuronal cells (*SI Appendix*, Fig. S13) (19). When BCCs were stimulated with Sema3A, the intensities of similar-sized bands were also increased (*SI Appendix*, Fig. S14 *A* and *B*). Furthermore, *MICAL3* knockdown using shRNA significantly decreased the intensities of the bands of the homodimers of CRMP2 (*SI Appendix*, Fig. S14*B*). It is likely that dimerization of CRMP2 is induced by Sema3A-stimulated activity of MICAL3 MO in BCCs. To examine whether the increase of dimerization of CRMP2 is induced by MICAL3-mediated H_2O_2 production, we used (−)-epigallocatechin gallate (EGCG) that is one of the green tea components and a selective inhibitor for MICAL MO (29, 34). In neuronal cells, EGCG treatment inhibits Sema3-induced axon repulsion (35). We found that Sema3A-induced dimerization of CRMP2 was decreased by EGCG treatment, similarly observed in *MICAL3* knockdown cells (*SI Appendix*, Fig. S15*A*). Moreover, EGCG treatment decreased tumor sphere-forming ability induced by Sema3A in a dose-dependent manner (*SI Appendix*, Fig. S15 *B* and *C*). Cell proliferation was not affected by EGCG treatment (*SI Appendix*, Fig. S16). These results further support the notion

that MICAL3-mediated H_2O_2 production is required for Sema3A-induced CRMP2 dimerization and tumor sphere formation in BCCs.
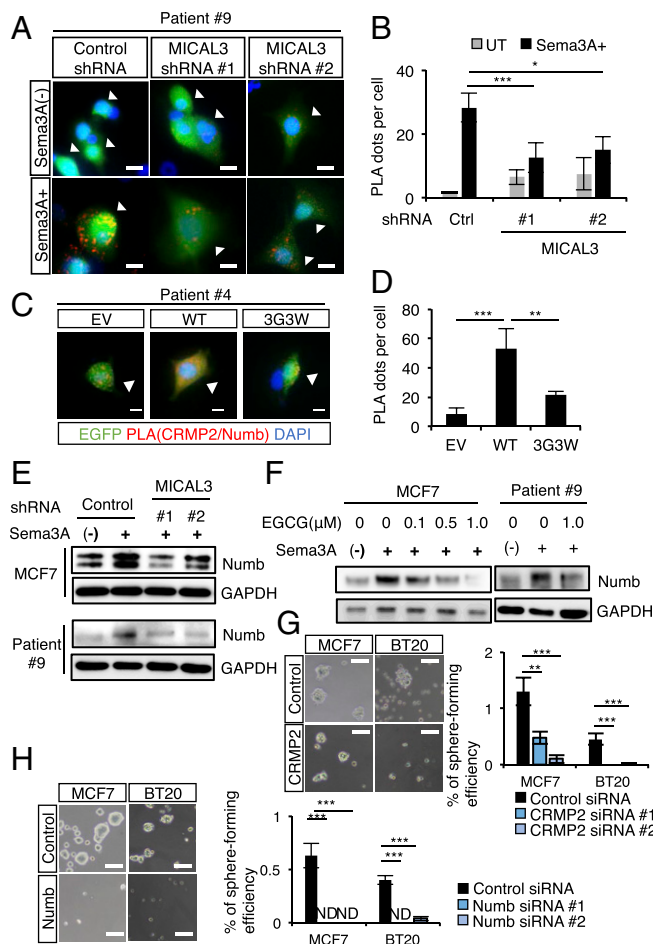
MO Domain of MICAL3 Is Required for Sema3A-Induced Interaction Between CRMP2 and Numb for Numb Stabilization. CRMP2 directly interacts with the amino-terminal fragment containing the phosphotyrosine binding domain of Numb during axon growth in the nervous system (20, 36). To examine whether CRMP2 interacts with Numb in BCCs, we used in situ PLA. We transfected MCF7 cells with *MICAL3* siRNA or transduced patient-derived BCCs with *MICAL3* shRNA and cultured the sorted NP1-positive cells in the presence or absence of Sema3A-containing medium for 24 h. The number of PLA dots was greatly increased in Sema3A-containing medium but not in the medium without Sema3A (Fig. 5 *A* and *B* and *SI Appendix*, Fig. S17 *A* and *B*). *MICAL3* knockdown significantly decreased the number of PLA dots in NP1-positive cells. To examine whether the MO domain of MICAL3 is required for the interaction between CRMP2 and Numb, BCCs were transiently transfected with cDNA constructs of MICAL3-WT or MICAL-3G3W in Sema3A-containing medium for 24 h. The PLA dots were observed much more in EGFP-positive MICAL3-WT–transfected cells than in EGFP-positive MICAL3-3G3W–transfected cells or empty vector (EV)-transfected cells (Fig. 5 *C* and *D* and *SI Appendix*, Fig. S18 *A* and *B*). These results suggest that Sema3A treatment induces MICAL3 MO domain-dependent interaction between CRMP2 and Numb in BCCs. To examine whether Sema3A signaling regulates Numb protein in BCCs, we analyzed the amount of Numb using immunoblotting. We found that stimulation with Sema3A increased the amount of Numb protein in BCCs (Fig. 5*E*). However, *MICAL3* knockdown or EGCG treatment inhibited Sema3A-stimulated accumulation of Numb protein in BCCs (Fig. 5 *E* and *F*). These data suggest that Sema3A signaling induces accumulation of Numb protein via MICAL3. In addition, *CRMP2* or *Numb* knockdown cells (*SI Appendix*, Fig. S19) showed greatly decreased tumor sphere formation cultured in Sema3A-containing medium (Fig. 5 *G* and *H*). All these results suggest that Sema3A treatment induces MICAL3 MO domain-dependent interaction between CRMP2 and Numb, leading to accumulation of Numb for sphere formation of BCCs.

Sema3A Induces Symmetric Division of NP1/Numb-Positive CSCs Mediated by MICAL3. To analyze symmetric–asymmetric cell division, we performed a cell pair assay using patient-derived BCCs (*SI Appendix*, Fig. S20). NP1-positive cells were sorted and cultured at a low density for 48 h in the medium with or without Sema3A. Single NP1-positive cells divided into pairs of daughter cells that were stuck together after 24 h. When cells were
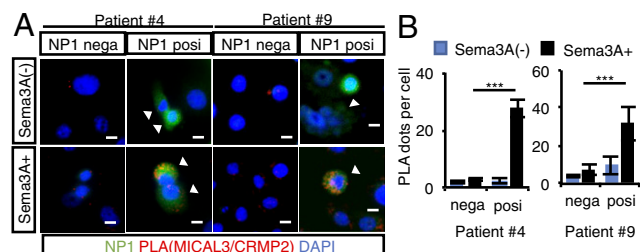
Fig. 4. MO activity of MICAL3 is required for Sema3A-induced CRMP2 dimerization and tumor sphere formation. (*A*) In situ PLA showed interactions between MICAL3 and CRMP2 in patient-derived BCCs treated with 200 ng/mL Sema3A for 24 h. After PLA, cells were further stained by an anti-NP1 antibody. White arrowheads indicate NP1-positive cells. (*B*) Quantification of the number of PLA dots per cell in NP1-positive (NP1^{posi}) and -negative (NP1^{nega}) cells. Twenty cells were counted for each condition. (Scale bar: 40 μm.) Data are shown as mean ± SD. ***$P < 0.001$ by Student's *t* tests.

Fig. 5. MO domain of MICAL3 is required for the interaction between CRMP2 and Numb for tumor sphere formation in human BCCs. (*A*) In situ PLA showed interactions between CRMP2 and Numb in NP1-positive patient-derived BCCs (patient 9) with 200 ng/mL Sema3A treatment for 24 h. PLA dots (red) indicate the interaction between CRMP2 and Numb by immuno-fluorescence. White arrowheads indicate control or GFP-positive *MICAL3* shRNA transfected cells. Ctrl, control shRNA. (Scale bar: 40 μm.) (*B*) Quanti-fication of the number of PLA dots per cell as shown in *A*. Twenty cells were counted for each condition. (*C*) The interaction between CRMP2 and Numb was greater in MICAL3-WT–transfected cells than in MICAL3-3G3W–transfected cells or in EV-transfected cells with Sema3A treatment for 24 h. PLA dots (red) indicate the interaction between CRMP2 and Numb by immunofluorescence. (Scale bar: 40 μm.) (*D*) Quantification of the number of PLA dots per cell as shown in *C*. Twenty cells were counted for each condi-tion. (*E*) Immunoblotting analysis of the expression of Numb in MCF7 cells or patient-derived BCCs transduced with control or *MICAL3* shRNA and stimu-lated with or without 200 ng/mL Sema3A for 6 h. (*F*) Immunoblotting analysis of the expression of Numb in MCF7 cells or patient-derived BCCs treated with EGCG at the indicated concentrations and stimulated with or without 200 ng/mL Sema3A for 6 h. Representative phase contrast images of tumor sphere formation by *CRMP2* knockdown (*G, Left*) or *Numb* knock-down (*H, Left*) in MCF7 cells or BT20 cells. (Scale bar: 100 μm.) Sema3A-induced tumor sphere formation was decreased by *CRMP2* knockdown (*G, Right*) or *Numb* knockdown (*H, Right*); n = 4. GAPDH was the loading control for immunoblotting. Data are shown as mean ± SD. *P < 0.05, **P < 0.01, ***P < 0.001 by Student's t tests.

immunostained with anti-NP1 and anti-Numb antibodies after the first cell division, we found that the NP1-positive cells were costained with the Numb protein on the cell membrane or in the cytoplasm (Fig. 6*A*). In cells that divided symmetrically, the NP1 and Numb proteins were strongly coexpressed and localized in both daughter cells. In cells that divided asymmetrically, the NP1

and Numb proteins were coexpressed in only one of the daughter cells, and neither protein was expressed at a detectable level in the other daughter cell. Numb proteins tended to be localized in the region where daughter cells were attached to each other. Interestingly, we found few if any daughter cells that were single positive for either NP1 or Numb. This finding suggests that Numb proteins are stabilized in NP1-positive CSCs but not in NP1-negative differentiated cells. When cells were cultured in Sema3A-containing medium, the frequency of symmetric cell division was greatly increased compared with control medium without Sema3A [untreated (UT)] (Fig. 6*B*). These results sug-gest that Sema3A treatment gives rise to more daughter CSCs by symmetric cell division than the control medium. *MICAL3* knockdown significantly decreased symmetric cell division in Sema3A-containing medium (Fig. 6 *C* and *D*) up to the levels of untreated cells. These findings suggest that Sema3A induces symmetric division of NP1/Numb-positive BCSCs and that MICAL3 plays critical roles for this process. From these results, we proposed that the Sema3/NP1/MICAL3/CRMP2/Numb sig-naling induces symmetric division of BCSCs. By inhibition of MICAL3 MO activity or knockdown of each component in the signaling pathway, the symmetric cell division may be inhibited, leading to reduction of BCSCs.

Evaluation of *Sema3*/NP1/*MICAL3* Expression in Breast Cancer Tissues. NP1 binds to four semaphorins, Sema3A, Sema3B, Sema3C, and Sema3D (15). To examine the significance of each semaphorin and patient outcome, we analyzed two gene expression profiles
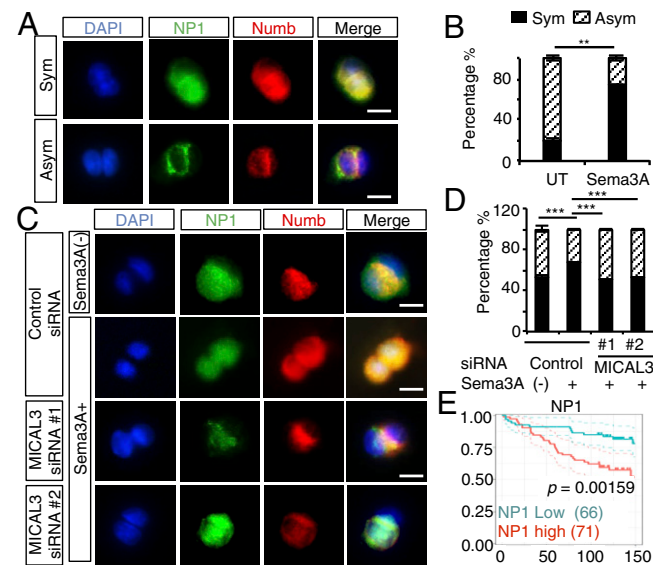
Fig. 6. MICAL3 plays important roles in Sema3A-induced symmetric cell division in breast CSCs. (*A*) Immunofluorescence for Numb and NP1 in cell pair assays showed colocalization of the two proteins in two daughter cells of the patient-derived BCSCs (patient 7) after symmetric (Sym) or asymmetric (Asym) cell division. The nuclei were stained with DAPI. (Scale bar: 40 μm.) (*B*) Quantification of the percentage of symmetric/asymmetric division in cell pair assays conducted in the absence (UT) or presence of 200 ng/mL Sema3A. Twenty cells were counted for each condition. Data are shown as mean ± SD. (*C*) Representative immunofluorescence images of cell pair assays using patient-derived BCSCs (patient 4). (Scale bar: 40 μm.) (*D*) Quantification of the percentage of symmetric/asymmetric division in cell pair assays con-ducted in the absence (−) or presence of 200 ng/mL Sema3A as shown in *C*. Twenty cells were counted for each condition. (*E*) Kaplan–Meier analysis of overall survival according to the NP1 expression levels in human breast cancer. Median of the area score (60) was used for cutoff values; n = 134. P value was calculated by log-rank test. Data are shown as mean ± SD. **P < 0.01, ***P < 0.001 by Student's t tests.

MEDICAL SCIENCES

www.manaraa.com

used for analysis of *MICAL3* in Fig. 2*B*. We found that *Sema3A* or *Sema3B*, but not *Sema3C* or *Sema3D*, showed significant coexpression with *MICAL3* (graphs surrounded by red frames in *SI Appendix*, Fig. S21). The expression levels of each *Sema3A*, *Sema3B*, or *Sema3D* alone did not show a significant association with patient outcome, while the expression levels of both *MICAL3* and *Sema3A* showed significantly worse outcomes in one gene expression profile. Expression levels of *Sema3C* showed an inverse correlation with those of *MICAL3* in one gene expression profile and high expression of *Sema3C* was associated with favorable prognosis in the other gene expression profile (graphs surrounded by blue frames in *SI Appendix*, Fig. S21). To examine the association between the expression levels of NP1 in tumor cells from breast cancer tissues and the outcome of the patients, we analyzed a tissue microarray of breast cancer tissues using antibodies against human NP1 (*SI Appendix*, Fig. S22*A*). Patients with high NP1 expression in tumor cells from their breast cancer tissues showed a significantly reduced overall survival rate compared with those with low/negative NP1 expression ($P = 0.0159$) (Fig. 6*E*). NP1 expression levels were higher in tumor cells from breast cancer tissues with a triple negative subtype than those in tumor cells from breast cancer tissues with the luminal A subtype ($P = 0.0179$, ANOVA with Dunnett's test) (*SI Appendix*, Fig. S22*B*). Immunofluorescence studies using antibodies against NP1 and Numb indicated the colocalization of NP1 and Numb in human breast cancer tissue samples (*SI Appendix*, Fig. S22*C*). Patients with higher levels of *NP1* in their breast cancer tissues showed significantly reduced relapse-free survival rate and distant metastasis-free survival rate compared with those with low *NP1* expression in their gene expression profiles (*SI Appendix*, Fig. S23) (37, 38). These results indicate that patients with breast cancer having high NP1 expression

levels in cancer tissues show poor prognosis. This is consistent with the notion that NP1 signaling increases the symmetric division of CSCs, resulting in their increased number and worse prognosis.

Discussion

In the current study, we discovered that the Sema3/NP1/MICAL3/CRMP2/Numb axis may be a specific mechanism for the maintenance of the symmetric division of self-renewing CSCs. To the best of our knowledge, this report shows that CSCs and neuronal cells utilize common signaling components for the maintenance of symmetric cell division and for repulsion cues or axonal growth, respectively. It is possible that the Sema3/NP1/MICAL3/CRMP2/Numb axis is active in a portion of the population in any subtype of breast cancer. Breast cancer patients with NP1^{high} staining in tumor tissues showed poor prognosis, and colocalization of Numb in breast cancer tissue samples from these patients was observed, consistent with the notion that NP1^{high} CSCs are responsible for relapse or drug resistance.

Materials and Methods

All human breast carcinoma specimens were obtained from the University of Tokyo Hospital, Minami Machida Hospital, Showa General Hospital, and Kanazawa Medical University. This study was approved by the institutional review boards of the Institute of Medical Science, University of Tokyo, the University of Tokyo Hospital, Minami Machida Hospital, Showa General Hospital, Kanazawa University, and Kanazawa Medical University. Written informed consent was obtained from all participants before inclusion in the study. Mice were handled according to the guidelines of the Institute of Medical Science, University of Tokyo. The experiments were approved by the committees for animal research at the Institute of Medical Science, University of Tokyo.

1. Torre LA, et al. (2015) Global cancer statistics, 2012. *CA Cancer J Clin* 65:87–108.
2. Kreso A, Dick JE (2014) Evolution of the cancer stem cell model. *Cell Stem Cell* 14: 275–291.
3. Neumüller RA, Knoblich JA (2009) Dividing cellular asymmetry: Asymmetric cell division and its implications for stem cells and cancer. *Genes Dev* 23:2675–2699.
4. Knoblich JA (2008) Mechanisms of asymmetric stem cell division. *Cell* 132:583–597.
5. Bajaj J, Zimdahl B, Reya T (2015) Fearful symmetry: Subversion of asymmetric division in cancer development and progression. *Cancer Res* 75:792–797.
6. Plaks V, Kong N, Werb Z (2015) The cancer stem cell niche: How essential is the niche in regulating stemness of tumor cells? *Cell Stem Cell* 16:225–238.
7. Hinohara K, Gotoh N (2010) Inflammatory signaling pathways in self-renewing breast cancer stem cells. *Curr Opin Pharmacol* 10:650–654.
8. Hinohara K, et al. (2012) ErbB receptor tyrosine kinase/NF-κB signaling controls mammosphere formation in human breast cancer. *Proc Natl Acad Sci USA* 109: 6584–6589.
9. Korkaya H, Liu S, Wicha MS (2011) Breast cancer stem cells, cytokine networks, and the tumor microenvironment. *J Clin Invest* 121:3804–3809.
10. Tominaga K, et al. (2017) Addiction to the IGF2-ID1-IGF2 circuit for maintenance of the breast cancer stem-like cells. *Oncogene* 36:1276–1286.
11. Sasahara A, et al. (2017) An autocrine/paracrine circuit of growth differentiation factor (GDF) 15 has a role for maintenance of breast cancer stem-like cells. *Oncotarget* 8:24869–24881.
12. Worzfeld T, Offermanns S (2014) Semaphorins and plexins as therapeutic targets. *Nat Rev Drug Discov* 13:603–621.
13. Tessier-lavigne M, Goodman C (1996) The molecular biology of axon guidance. *Science* 274:1123–1133.
14. Neufeld G, Sabag AD, Rabinovicz N, Kessler O (2012) Semaphorins in angiogenesis and tumor progression. *Cold Spring Harb Perspect Med* 2:a006718.
15. Neufeld G, Kessler O (2008) The semaphorins: Versatile regulators of tumour progression and tumour angiogenesis. *Nat Rev Cancer* 8:632–645.
16. Hung R-J, Terman JR (2011) Extracellular inhibitors, repellents, and semaphorin/plexin/MICAL-mediated actin filament disassembly. *Cytoskeleton (Hoboken)* 68: 415–433.
17. Zhou Y, Gunput R-AF, Adolfs Y, Pasterkamp RJ (2011) MICALs in control of the cytoskeleton, exocytosis, and cell death. *Cell Mol Life Sci* 68:4033–4044.
18. Schmidt EF, Shim S-O, Strittmatter SM (2008) Release of MICAL autoinhibition by semaphorin-plexin signaling promotes interaction with collapsin response mediator protein. *J Neurosci* 28:2287–2297.
19. Morinaka A, et al. (2011) Thioredoxin mediates oxidation-dependent phosphorylation of CRMP2 and growth cone collapse. *Sci Signal* 4:ra26.
20. Schmidt EF, Strittmatter SM (2007) The CRMP family of proteins and their role in Sema3A signaling. *Adv Exp Med Biol* 600:1–11.
21. Shen Q, Zhong W, Jan YN, Temple S (2002) Asymmetric Numb distribution is critical for asymmetric cell division of mouse cerebral cortical stem cells and neuroblasts. *Development* 129:4843–4853.
22. Shimojo H, Ohtsuka T, Kageyama R (2011) Dynamic expression of notch signaling genes in neural stem/progenitor cells. *Front Neurosci* 5:78.
23. Noatynska A, Tavernier N, Gotta M, Pintard L (2013) Coordinating cell polarity and cell cycle progression: What can we learn from flies and worms? *Open Biol* 3:130083.
24. Dzierzak E, Enver T (2008) Stem cell researchers find their niche. *Development* 135: 1569–1573.
25. Zhong W, Chia W (2008) Neurogenesis and asymmetric cell division. *Curr Opin Neurobiol* 18:4–11.
26. Ablett MP, Singh JK, Clarke RB (2012) Stem cells in breast tumours: Are they ready for the clinic? *Eur J Cancer* 48:2104–2116.
27. Okada T, et al. (2015) The Rho GTPase Rnd1 suppresses mammary tumorigenesis and EMT by restraining Ras-MAPK signalling. *Nat Cell Biol* 17:81–94.
28. Al-Hajj M, Wicha MS, Benito-Hernandez A, Morrison SJ, Clarke MF (2003) Prospective identification of tumorigenic breast cancer cells. *Proc Natl Acad Sci USA* 100: 3983–3988.
29. Terman JR, Mao T, Pasterkamp RJ, Yu H-H, Kolodkin AL (2002) MICALs, a family of conserved flavoprotein oxidoreductases, function in plexin-mediated axonal repulsion. *Cell* 109:887–900.
30. Hung R-J, et al. (2010) Mical links semaphorins to F-actin disassembly. *Nature* 463: 823–827.
31. Grigoriev I, et al. (2011) Rab6, Rab8, and MICAL3 cooperate in controlling docking and fusion of exocytotic carriers. *Curr Biol* 21:967–974.
32. Zhou Y, et al. (2011) MICAL-1 is a negative regulator of MST-NDR kinase signaling and apoptosis. *Mol Cell Biol* 31:3603–3615.
33. Söderberg O, et al. (2006) Direct observation of individual endogenous protein complexes in situ by proximity ligation. *Nat Methods* 3:995–1000.
34. Nadella M, Bianchet MA, Gabelli SB, Barrila J, Amzel LM (2005) Structure and activity of the axon guidance protein MICAL. *Proc Natl Acad Sci USA* 102:16830–16835.
35. Pasterkamp RJ, et al. (2006) MICAL flavoprotein monooxygenases: Expression during neural development and following spinal cord injuries in the rat. *Mol Cell Neurosci* 31: 52–69.
36. Nishimura T, et al. (2003) CRMP-2 regulates polarized Numb-mediated endocytosis for axon growth. *Nat Cell Biol* 5:819–826.
37. Wang Y, et al. (2005) Gene-expression profiles to predict distant metastasis of lymph-node-negative primary breast cancer. *Lancet* 365:671–679.
38. Loi S, et al. (2010) PIK3CA mutations associated with gene signature of low mTORC1 signaling and better outcomes in estrogen receptor-positive breast cancer. *Proc Natl Acad Sci USA* 107:10208–10213.

Tominaga et al.

www.manaraa.com